RSC Advances

PAPER

View Article Online
View Journal | View Issue

Cite this: *RSC Adv.*, 2026, **16**, 24627

Curcumin release from hydrogels incorporated with turmeric extract–cyclodextrin complexes for wound dressing applications

Rawita Morarad,[a] Pennapa Karawak,[a] Pranita Meepean,[a] Natawan Sritapanya,[a] Pattaraphorn Panomai,[a] Niti Yongvanich[b] and Pimpon Uttayarat*[a]

Curcumin, the major bioactive compound of turmeric, exhibits potent antioxidant and anti-inflammatory activities with significant therapeutic potential for wound healing. However, its clinical use is hindered by inherently poor water solubility. In this study, cyclodextrin (CD) inclusion complexes were prepared with turmeric extract (TE) to enhance the aqueous solubility and release of curcumin from hydrogels intended as active wound dressings. The TE-to-CD ratio was systematically varied from 10–80% (w/w), yielding complexes designated as 10TECD–80TECD formulations. Formulations below 20TECD exhibited superior aqueous solubility while retaining antioxidant activity. SEM analysis showed a morphological transition from large (~5 μm) to smaller (~1 μm) flake-like particles in formulations below 40TECD. The TECD complexes were subsequently incorporated into hydrogel sheets prepared from 3–8% (w/v) poly(vinyl alcohol) (PVA), which were crosslinked by freeze-thaw cycling followed by electron beam irradiation. Curcumin release was inversely related to PVA concentration, with the lowest concentration producing the most porous matrix structure and greatest surface area, thereby facilitating the highest release. The optimized formulation, consisting of a 3PVA hydrogel loaded with 20TECD, achieved a cumulative curcumin release of 13.25% within 6 h, with release characteristics consistent with Fickian diffusion kinetics. The system exhibited no cytotoxicity and also showed anti-inflammatory activity as confirmed by nitric oxide inhibition assay. These findings highlight the potential of TECD-loaded PVA hydrogels as effective bioactive wound dressing materials for curcumin delivery.

Received 27th January 2026
Accepted 4th May 2026

DOI: 10.1039/d6ra00713a

rsc.li/rsc-advances

1. Introduction

Turmeric (*Curcuma longa* L.) is one of the most popular medicinal herbs belonging to the Zingiberaceae family. It is cultivated in tropical and subtropical regions, primarily in Asian countries, and has been regarded as a traditional medicine in both Ayurvedic and Chinese systems for centuries.[1] The main bioactive components of turmeric are curcuminoids, which include curcumin, demethoxycurcumin, and bisdemethoxycurcumin.[2] The U.S. Food and Drug Administration has designated curcumin and related curcuminoids as "Generally Recognized as Safe" (GRAS), supporting their potential for clinical applications.[3] Among the three curcuminoids, curcumin represents the major component, comprising up to 75% of the total curcuminoid content. Owing to its diverse biological activities, including antibacterial, anti-inflammatory, antioxidant, antimutagenic, and anticancer properties, curcumin has been applied in various medical treatments, such as wound healing, oral supplementation, and topical therapeutic formulations.[4,5] The chemical structures of these compounds are shown in Scheme 1A.

Curcumin, chemically known as diferuloylmethane ($C_{21}H_{20}O_6$), is a low molecular weight polyphenol (368.38 g mol^{-1}) with a hydrophobic structure. It is a symmetrical molecule in which the two keto groups can undergo keto–enol tautomerization, interconverting between ketone and alcohol forms. The enol form predominates in the solid state and in alkaline aqueous solutions, while the keto form is favored in acidic and neutral aqueous environments.[6] Between these two tautomers, the enol form of curcumin provides higher antioxidant activity.[7] However, the clinical application of curcumin is limited by its poor water solubility and low bioavailability, as it undergoes rapid degradation during first-pass metabolism.[8,9] Over the years, several strategies have been developed to overcome these limitations, including nanoparticle-based formulations (such as silica-based systems and single-walled carbon nanotubes) and cyclodextrin complexation.[10] Among these, cyclodextrin complexation has been extensively studied due to its simple preparation and low cost. This method effectively enhances curcumin solubility, which in turn improves its

[a]*Nuclear Technology Research and Development Center, Thailand Institute of Nuclear Technology (Public Organization), Nakhon Nayok, 26120, Thailand. E-mail: pimponu@tint.or.th*

[b]*Department of Materials Science and Engineering, Faculty of Engineering and Industrial Technology, Silpakorn University, Nakhon Pathom, 73000, Thailand*

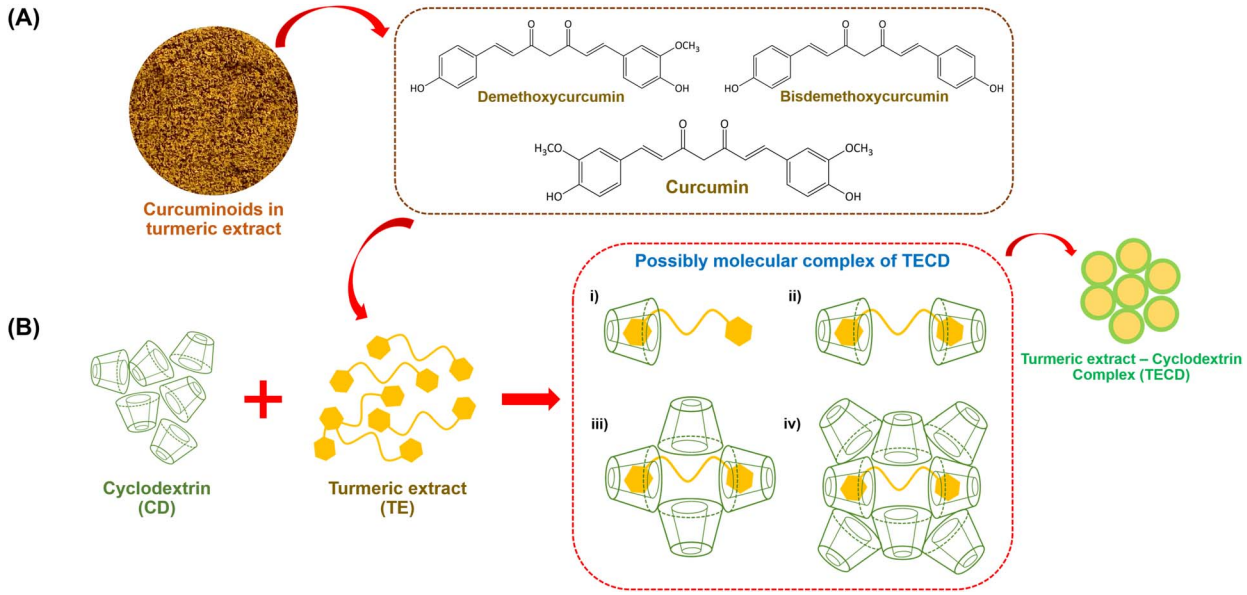

Scheme 1 Chemical structures and supramolecular assembly concepts: (A) chemical structures of the three principal curcuminoids found in turmeric; and (B) proposed structural evolution of turmeric extract–cyclodextrin (TECD) complexes.

gastrointestinal absorption and facilitates its transportation to target tissues.[10]

Cyclodextrins (CDs) are cyclic oligosaccharides characterized by a hydrophobic inner cavity and a hydrophilic exterior.[11] This unique structure enables their widespread pharmaceutical application as delivery vehicles for poorly soluble drugs such as curcumin,[12,13] ketoconazole,[14,15] and ibuprofen,[16,17] thereby enhancing their drug stability, solubility, bioavailability, and release efficiency.[18] Curcumin is encapsulated within the inner cavity of CDs *via* host–guest interactions mediated by non-covalent forces, namely van der Waals forces and hydrophobic interactions.[19] The most common molar ratios of curcumin and CD complexes are 1 : 1 and 1 : 2 stoichiometry, in which one curcumin molecule is included within the cavity of one or two CD molecules, respectively. However, higher stoichiometry complexes involving more than two CD molecules could also occur through supramolecular self-assembly, resulting in large molecular aggregates stabilized by noncovalent interactions (Scheme 1B).[12,20]

Hydrogels are three-dimensional hydrophilic polymer networks with a high capacity to absorb and retain water, often exceeding 90% of their total weight.[21] Due to their high-water content, hydrogels exhibit flexibility and softness, making them particularly suitable for wound dressing applications. Compared with conventional wound dressings such as gauze, bandage, or cotton wool, hydrogels offer several advantages, including the ability to maintain a moist wound environment, promote cell migration and proliferation, and serve as carriers for bioactive agents.[22] Poly(vinyl alcohol) (PVA), a synthetic water-soluble polymer, is one of the most widely used materials for wound dressing due to its biocompatibility, biodegradability, non-toxicity, low cost, and ease of processing.[23] PVA hydrogels can be formed through physical, chemical, or radiation-induced crosslinking mechanisms.[24] Physical crosslinking *via* freeze-thaw cycles provides a simple and convenient approach for converting aqueous PVA solutions into three-dimensional (3D) networks; however, the resulting hydrogels are not permanent and may revert to their initial solution state. In contrast, chemical and radiation-induced crosslinking produce permanent 3D networks. Radiation-induced crosslinking is especially advantageous, as it avoids the need for chemical crosslinkers and eliminates concerns related to residual toxic agents that may leach out and cause irritation or systemic toxicity.[24] By combining physical and radiation-induced crosslinking approaches, hydrogels with dual network structures can be formed, resulting in enhanced mechanical properties.[25]

Hydrogels loaded with curcumin enable localized drug release at the wound site, thereby enhancing therapeutic efficacy. Building on these advantages, various curcumin-hydrogel composite systems have been developed for tissue regeneration and wound dressing applications.[26–28] Zhang *et al.* (2025) reported a thermoresponsive curcumin-loaded chitin/lignin micelle hydrogel with tissue-adhesive properties for wound regeneration, achieving suture-free wound closure and enhanced healing through reduced inflammatory responses.[26] Similarly, Pan *et al.* (2021) developed curcumin-loaded self-healing hydrogels with dynamic boronic ester linkages, which triggered multi-responsive curcumin release and promoted cell-layer wound repair.[27] Zhao *et al.* (2019) fabricated chitosan–alginate dressings incorporating CD-curcumin inclusion complexes, achieving sustained curcumin release, enhanced antioxidant activity, and accelerated wound healing in animal models.[28] Despite growing interest in curcumin-based therapeutics, previous studies have predominantly focused on purified curcumin, whereas hydrogels incorporating turmeric extract (TE) complexed with cyclodextrin (CD) to improve the solubility of naturally derived curcumin remain largely

unexplored. Developing such systems offers a more sustainable and cost-effective alternative without compromising therapeutic efficacy.

In this work, curcumin was directly extracted from turmeric, a locally abundant agricultural resource in Thailand, which contains all three curcuminoid analogs, including curcumin, demethoxycurcumin, and bisdemethoxycurcumin. All these analogs provide biological activities despite different potencies, and the synergistic activity of all constituents determines the resultant biological activity of the extract. The aqueous solubility of TE and its release performance from hydrogels were subsequently enhanced through the formation of inclusion complexes with CD. Unlike previous studies that typically rely on purified commercial curcumin, we systematically varied the TE-to-CD ratio to obtain a series of complexes ranging from supramolecular assemblies to small-molecule inclusion complexes. The resulting TECD complexes were then incorporated into PVA hydrogels, with both TECD formulation and hydrogel matrix concentration tuned to determine their roles in curcumin loading and diffusion. We demonstrate that hydrogels with larger surface area and more porous matrix structures facilitate more efficient curcumin release, while increasing PVA concentration strengthens the network but limits diffusion. Together, these investigations establish a rational formulation pathway for improving the delivery of curcumin and other poorly soluble natural products using CD-based complexes, thereby validating the system's potential for advanced wound dressing applications.

2. Materials and method

2.1. Materials

Turmeric powder (100%) was kindly donated by Charoensuk Pharma Supply Co., Ltd (CPS), Thailand. β-Cyclodextrin (CD; $C_{42}H_{70}O_{35}$; ≥97%, Mw: 1134.98 g mol^{-1}), poly(vinyl alcohol) (PVA; ≥99% hydrolyzed, Mw: 89 000–98 000 g mol^{-1}), and Dulbecco's phosphate buffered saline (DPBS; liquid, sterile-filtered), 3-(4,5-dimethylthiazol-2-yl)-2,5-diphenyltetrazolium bromide (MTT), minimum essential medium (MEM), fetal bovine serum (FBS), L-glutamine, penicillin-streptomycin, and dimethyl sulfoxide (DMSO) were purchased from Sigma-Aldrich, USA. Mouse fibroblasts (NCTC clone 929, lot# 62727942) were purchased from ATCC (Manassas, VA, USA). Reference materials including high-density polyethylene (HDPE) and polyurethane for the MTT assay were obtained from Hatano (Kanagawa, Japan). Methanol (MeOH; HPLC-gradient grade; VWR Chemicals; USA) and ethanol (EtOH; gradient grade for liquid chromatography; Sigma-Aldrich; USA) were used for HPLC measurements. Ethanol (EtOH; absolute, analytical grade; EMSURE, USA) was used as a solvent. The 2,2′-azino-bis(3-ethylbenzothiazoline-6-sulfonic acid) diammonium salt (ABTS; ≥98%), potassium persulfate ($K_2S_2O_8$; ≥99.0%), and L-ascorbic acid (≥98%) were purchased from Sigma-Aldrich, USA, and used in the antioxidant assay. Sodium nitroprusside dihydrate (SNP; Sigma Aldrich), sulphanilamide (99%, Loba Chemie), *N*-(1-naphthyl) ethylenediamine dihydrochloride (NED; Sigma Aldrich), and phosphoric acid (H_3PO_4; Sigma Aldrich) were used as reagents in anti-inflammatory assay. All chemicals were of analytical grade. Deionized water (DI water) was used in all experiments unless otherwise stated.

2.2. Turmeric extraction procedure

The turmeric powder was extracted using the Soxhlet extraction (SE) technique. Briefly, 10 g of turmeric powder was placed in a 33 × 94 mm extraction thimble (cellulose thimble, single thickness; Whatman) and extracted using SE with 350 mL of 70% (v/v) EtOH as the solvent at 100 °C for 5 h. The solvent was then evaporated using a rotary evaporator (Heidolph, Schwabach, Germany) at a rotational speed of 80 rpm, a pressure of 100 mbar, and a temperature of 45 °C for 1 h. The concentrated extract was subsequently frozen at −80 °C for 48 h and dried using a lyophilizer (Labconco, Missouri, USA) for 72 h. Finally, the turmeric extract powder (TE) was obtained and weighed to calculate the extraction yield (%). The TE powder was stored at −20 °C, protected from light, until further use.

2.3. Preparation of turmeric extract–cyclodextrin complexes (TECD)

This method was modified from the previously reported protocol by Yallapu *et al.* (2010).[12] CD (40 mg) was dissolved in 8 mL of DI water and stirred at 400 rpm for 10 min to obtain a homogeneous solution. TE was separately dissolved in 0.5 mL of EtOH at TE concentrations of 10%, 20%, 40%, 60%, and 80% (w/w) relative to CD (TE : CD). The proportions of each component are listed in Table 1. The TE solutions were then slowly added dropwise to the CD solution and stirred at 400 rpm for 12 h. The resulting samples were centrifuged at 1000 rpm for 10 min. The supernatant was frozen at −80 °C for 24 h and subsequently dried with a lyophilizer for 72 h to obtain TECD powder. The powder was weighed to calculate the % yield and stored at −20 °C, protected from light, until further use.

2.4. Characterization of TECD

2.4.1. Scanning electron microscope (SEM). The morphology of TE, CD, and TECD powders was investigated using a scanning electron microscope (SEM; MIRA3, Tescan, Brno, Czech Republic) operated at an accelerating voltage of 5 kV and magnifications of 1000× and 10 000×. All samples were coated with gold prior to testing to enhance electrical conductivity.

2.4.2. FTIR analysis. The functional groups of TE, CD, and TECD powders were analyzed using Fourier transform infrared spectroscopy (FTIR; INVENIO, Bruker, Karlsruhe, Germany) in the attenuated total reflectance (ATR)-FTIR transmission mode over a wavenumber range of 550–4000 cm^{-1} with 32 scans.

2.4.3. Curcumin content. A rapid screening method for determining curcumin content in TE and TECD was established using a UV-VIS spectrophotometer (SPECTROstar Nano, BMG LABTECH, Offenburg, Germany). Samples (1 mg) were dissolved in 1 mL EtOH and diluted with phosphate buffer (pH 7.4) until homogeneous solutions were obtained at a final concentration of 0.1 mg mL^{-1}. Aliquots of 100 μL were transferred to a 96-well plate, and absorbance was measured. The curcumin content was

Table 1 Formulation compositions for TECD inclusion complex preparation

Formulation	Initial TE (mg)	Initial CD (mg)	TE : CD (wt%)	Approximate molar ratio (TE : CD)
10TECD	4	40	10	1 : 20
20TECD	8	40	20	1 : 10
40TECD	16	40	40	1 : 5
60TECD	24	40	60	1 : 3
80TECD	32	40	80	1 : 2

quantified using a standard calibration curve. For precise quantification, curcumin content in TE and TECD was also measured using High-Performance Liquid Chromatography (HPLC). The HPLC system (Waters Alliance e2695 HPLC Separation Module, Massachusetts, USA) equipped with a photodiode array detector (Waters 2998 PDA, USA) and a C18 reverse-phase column (150 mm × 4.6 mm × 5 μm; Agilent ZORBAX Eclipse Plus, USA) was employed. Detection was performed at a wavelength of 425 nm. The mobile phase consisted of 85% (v/v) EtOH, delivered at a flow rate of 0.8 mL min^{-1} under isocratic elution at 30 °C. Samples (10 μL) were automatically injected into the HPLC after filtration through a 0.45 μm nylon syringe filter. The retention time of curcumin was approximately 7 min. The curcumin content was quantified using a standard curve over a concentration range of 0.01–0.2 mg mL^{-1}.

2.4.4. Water solubility testing. The maximum water solubility of TECD powders was investigated by weighing 1 mg of each TECD formulation into a microtube, followed by the gradual addition of DI water in 50 μL increments until the TECD was completely dissolved. The total volume of DI water required for complete dissolution was recorded.

2.5. ABTS antioxidant assay

The $ABTS^{\bullet+}$ working solution was prepared by mixing 7 mM ABTS solution with 4.95 mM $K_2S_2O_8$ and kept in the dark at room temperature for 16 h. Prior to use, the $ABTS^{\bullet+}$ solution was diluted with MeOH to obtain an absorbance value of 0.70 ± 0.03 at 734 nm. For the assay, 50 μL of sample solution at various concentrations was mixed with 150 μL of $ABTS^{\bullet+}$ solution in a 96-well plate and incubated for 10 min at room temperature in the dark. Absorbance was measured using a microplate reader at 734 nm. Radical scavenging activity (%) was calculated using eqn (1) as follows:

$$\text{ABTS radical scavenging}(\%) = \left(\frac{A_{\text{ABTS}} - A_{\text{sample}}}{A_{\text{ABTS}}}\right) \times 100 \quad (1)$$

where A_{ABTS} represents the absorbance of the $ABTS^{\bullet+}$ and A_{sample} represents the absorbance of the sample. Ascorbic acid was used as a positive control. The antioxidant capacity was reported as IC_{50} (mg mL^{-1}). All experiments were performed in triplicate.[29]

2.6. Preparation of PVA hydrogel

PVA powder (3, 5, and 8 g) was dissolved in 100 mL of boiling water and stirred with a magnetic stirrer for 30 min. Then, 25 mL of PVA solution was transferred into a 12 × 12 cm^2 square Petri dish and subjected to two freeze-thaw cycles by freezing at −20 °C for 24 h and thawing at room temperature for 2 h. After that, the samples were irradiated using EB irradiation generated by an electron accelerator (MB10-50) at a dose of 25 kGy at the Gem Irradiation Center, Thailand Institute of Nuclear Technology (Public Organization).

2.7. Characterization of PVA hydrogel

2.7.1. Gel fraction. According to Chiangnoon *et al.* (2023),[30] hydrogel samples were cut into two halves of approximately equal weight. One half was boiled in DI water to remove free PVA molecules. Both treated and untreated halves were then dried at 60 °C until a constant weight was achieved. The gel fraction percentage (%) was calculated using eqn (2) as follows:

$$\text{Gel fraction}(\%) = \frac{W_d}{W_0} \quad (2)$$

where W_d represents the weight of the insoluble fraction of the dried hydrogel after boiling, and W_0 represents the initial weight of the dried hydrogel. All experiments were performed in triplicate.

2.7.2. Swelling ratio. The hydrogel samples were first cut and rinsed with DI water to remove free PVA molecules, and then fully immersed in water. The swollen hydrogels were weighed at 24 h. The swelling ratio was determined according to eqn (3):

$$\text{Swelling ratio} = \frac{W_s}{W_i} \quad (3)$$

where W_s represents the swollen weight of the hydrogel and W_i represents the initial weight of the hydrogel after irradiation.[30] All experiments were performed in triplicate.

2.7.3. Mechanical properties testing. Hydrogel sheets were cut into dumbbell-shaped specimens according to ASTM D-1822, with a gauge length of 9.45 mm and a width of 3.20 mm. Tensile tests were conducted using a texture analyzer (Lloyd LS1, AMETEK, Largo, FL, USA) equipped with a 50 N load cell. Both ends of the samples were gripped and stretched at a crosshead speed of 50 mm min^{-1}. The tensile strength, elongation at break, and Young's modulus were recorded. Each test was performed in quintuplicate.

2.7.4. Scanning electron microscope (SEM). The surface and cross-sectional morphologies of PVA hydrogels were investigated using a scanning electron microscope operated at an accelerating voltage of 5 kV and magnifications of 500× and 1000×. For cross-sectional analysis, lyophilized hydrogels were

immersed in liquid nitrogen for 5 min, cold-fractured, and coated with gold to enhance conductivity.

2.8. Incorporation of TECD in hydrogels

The hydrogels were cut into 3 × 3 cm^2 squares and partially dehydrated at 37 °C for 2 h to remove approximately 10% of their moisture content based on weight loss. Fresh TECD solutions were prepared by dissolving TECD in 500 μL of DI water and sonicated for 10 min to obtain homogeneous solutions. Then, the TECD solution was added to the partially dehydrated hydrogels and kept in a closed container at room temperature for 4 h. The full absorption of TECD into the PVA hydrogel was assessed through both visual and tactile observation and was considered complete when no visible liquid remained on the hydrogel surface. To further confirm this, a dry wiper was gently contacted with the hydrogel surface post-absorption. The absence of any moisture transfer to the wiper confirmed that no residual TECD solution remained on the hydrogel surface, validating complete absorption into the matrix (Fig. S1).

2.9. *In vitro* TECD release from irradiated PVA hydrogel and release kinetics

Standard curcumin was dissolved in EtOH at a concentration of 1 mg mL^{-1} and subsequently diluted with phosphate buffer using 2-fold serial dilutions to obtain a range of concentrations. Absorbance was measured using a UV-VIS spectrophotometer at a wavelength of 426 nm, and a calibration curve was constructed by plotting standard curcumin concentrations (x-axis) against their corresponding absorbance values (y-axis).

TECD-loaded PVA hydrogel samples were immersed in 5 mL of phosphate buffer (pH 7.4) to simulate physiological conditions and incubated at 37 °C under shaking at 100 rpm. At predetermined time intervals, aliquots were withdrawn and replenished with fresh PBS to maintain sink conditions. The curcumin content of each aliquot was quantified by UV-VIS spectroscopy at 426 nm against a pre-established calibration curve. The cumulative percentage of curcumin released was calculated using eqn (4):

$$\%\ \text{Curcumin released} = \left(\frac{\text{amount of curcumin released}}{\text{initial curcumin amount loaded in hydrogel}}\right) \times 100 \quad (4)$$

The release kinetics of curcumin from the hydrogels were analyzed using the Korsmeyer–Peppas model, a widely applied model for describing drug release mechanisms from polymeric systems. This model relates the cumulative fraction of drug released to time as a power-law function, as expressed in eqn (5):

$$\frac{M_t}{M_\infty} = kt^n \quad (5)$$

where M_t represents the amount of curcumin released at time t (μg), M_∞ represents the total amount of curcumin released (μg), k represents the release rate constant of the system (h^{-n}), and n is the diffusion scaling exponent, which indicates the predominant release mechanism.[31]

2.10. Cytotoxicity

The cytotoxicity of 20TECD-loaded PVA hydrogel, 20TECD solution alone, and TE was evaluated using the MTT assay. Prior to hydrogel incorporation, the 20TECD solution was filter-sterilized through a 0.22 μm nylon membrane under aseptic conditions. The hydrogels were cut into 3 × 3 cm^2 pieces and extracted in complete MEM supplemented with 10% FBS, 4 mM L-glutamine, and 100 IU/mL penicillin-streptomycin at a ratio of 0.1 g mL^{-1}, in accordance with ISO 10993-12.[32] Extraction was carried out in an incubator at 37 °C for 24 h under orbital shaking at 80 rpm. Polyurethane and HDPE served as positive (cytotoxic) and negative (non-cytotoxic) controls, respectively, while complete medium alone was used as the blank control.

The mouse fibroblasts, or L929, cells were seeded at a density of 1 × 10^4 cells per well in a 96-well plate containing complete MEM and incubated at 37 °C in a humidified atmosphere of 5% CO_2 for 24 h. Following this initial incubation, the cells were exposed to either assay medium or extraction medium for a further 24 h. The medium was then aspirated and replaced with freshly prepared MTT solution (1 mg mL^{-1}), and the cells were incubated for an additional 3 h to facilitate formazan crystal formation. Subsequently, isopropanol (100 μL) was added to each well to dissolve the formazan crystals, and the optical density was recorded at 570 nm using a microplate reader. Cell viability was expressed as a percentage according to eqn (6):

$$\%\ \text{Cell viability} = \frac{\text{Abs}_{\text{extract}}}{\text{Abs}_{\text{blank}}} \times 100 \quad (6)$$

where the $\text{Abs}_{\text{extract}}$ is the absorbance from wells treated with assay or extraction media, and $\text{Abs}_{\text{blank}}$ is from wells with blank control. All experiments were conducted in quintuplicates.

2.11. Nitric oxide radical scavenging assay

The nitric oxide (NO) activity was assessed using a cell-free system based on the Griess reaction, as described by Suksungworn *et al.* (2020).[33] Briefly, 100 μL of SNP (10 mM) in PBS was mixed with 100 μL of the sample at various concentrations and incubated at 25 °C for 60 min under light. Following incubation, 100 μL of Griess reagent, consisting of 1% sulphanilamide, 0.1% NED, and 2% H_3PO_4 was added to the mixture. The absorbance of the resulting nitrite was measured at 546 nm using a microplate reader. The percentage of NO inhibition was determined by eqn (7):

$$\text{NO radical scavenging}(\%) = \left(\frac{A_{\text{control}} - A_{\text{sample}}}{A_{\text{control}}}\right) \times 100 \quad (7)$$

where A_{control} represents the absorbance of the reaction mixture without the sample and A_{sample} represents the absorbance in the presence of the sample. All experiments were performed in triplicate.

2.12. Statistical analysis

GraphPad Prism version 10 (GraphPad Software, San Diego, CA, USA) with the one-way ANOVA followed by Tukey's post hoc test was used for the statistical analysis. The data were expressed as the mean ± standard deviation (SD). Statistical significance was assessed as p-value < 0.05, and high significance was defined as p-value < 0.01.

3. Results and discussion

3.1. Turmeric extract characterization

Using Soxhlet extraction, a dark orange-red extract powder was obtained with an extraction yield of 23.02% (w/w). The HPLC chromatogram and UV-VIS spectrum provided distinct fingerprints for curcumin, enabling its reliable identification and quantification in TE.

The HPLC chromatogram (Fig. 1A) showed a sharp and well-defined peak at a retention time of 2.135 min, which matched the characteristic retention time for pure curcumin. This peak served as a reference fingerprint, confirming the presence of curcumin in the sample. The narrow and symmetrical nature of the peak indicated high purity and minimal interference from other compounds. Quantification based on the area under the curve demonstrated that the crude extract contained 16.6% (w/w) curcumin.

The UV-VIS spectrum of curcumin typically features a strong absorption band in the range of 420–430 nm, attributable to the conjugated diketone chromophore within the molecule.[34] As shown in Fig. 1B, TE exhibited a characteristic absorbance peak centered at 426 nm, providing an additional fingerprint for curcumin and related curcuminoids. Based on absorbance values and a standard calibration curve, TE showed a high apparent curcumin content of 40.5% (w/w). The 2.4-fold higher value obtained by UV-VIS compared to HPLC can be attributed to its non-selective response to all conjugated chromophores present in the extract, including demethoxycurcumin, bisdemethoxycurcumin, and other phenolic co-extractives, which absorb at similar wavelengths and therefore inflate absorbance-based estimates.[35] Although UV-VIS spectroscopy lacks the chromatographic resolution required to distinguish individual curcuminoids, it offers several practical advantages, including simplicity, low cost, rapid analysis, and high throughput with minimal sample preparation. These advantages make UV-VIS a useful tool for preliminary evaluation of total chromophoric content and for routine quality screening during formulation development.[36]

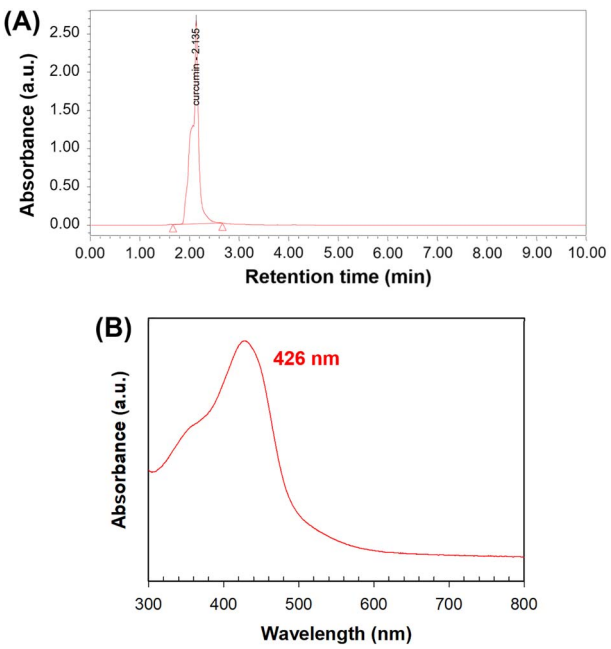

Fig. 1 Characterization of curcumin fingerprint in TE: (A) HPLC chromatogram showing the retention time of curcumin, and (B) UV-VIS spectrum showing the characteristic absorption peak at 426 nm.

Table 2 Complexation yield and water solubility of TECD complexes

Sample	% Yield	Water solubility (mg mL^{-1})
CD	87.78	>10
10TECD	84.55	3.25 ± 0.05
20TECD	72.50	1.40 ± 0.10
40TECD	60.00	1.14 ± 0.04
60TECD	58.75	1.00 ± 0.00
80TECD	59.03	1.00 ± 0.00

3.2. Characterization of TECD and its curcumin content

The TECD complexation yield exhibited a clear inverse relationship with TE loading, and a similar trend was observed in previous work.[13] The % yield decreased from 84.55% for 10TECD and reached a constant value of approximately 60% for the 40TECD formulation and higher TE loadings (Table 2). Statistical analysis indicated no significant differences among the % yield of 40TECD, 60TECD, and 80TECD formulations (p > 0.05), suggesting that the cyclodextrin inclusion capacity was saturated at TE : CD ratios above 40 wt%. This constant yield implies that TE in excess of this threshold cannot be effectively complexed and remains as free extract, which is lost during the process.

The curcumin content in TECD was measured by both UV-VIS and HPLC. Quantitative HPLC analysis showed that curcumin content in TECD formulations increased linearly with

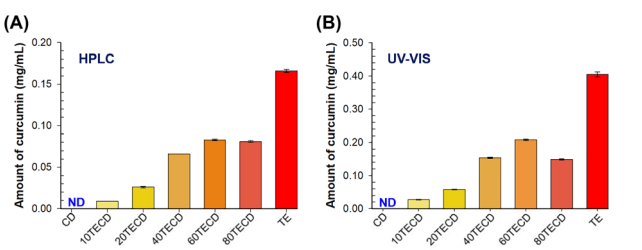

Fig. 2 Curcumin content in TE and TECD complexes: (A) quantification by HPLC; and (B) UV-VIS spectroscopy. ND = Not detected.

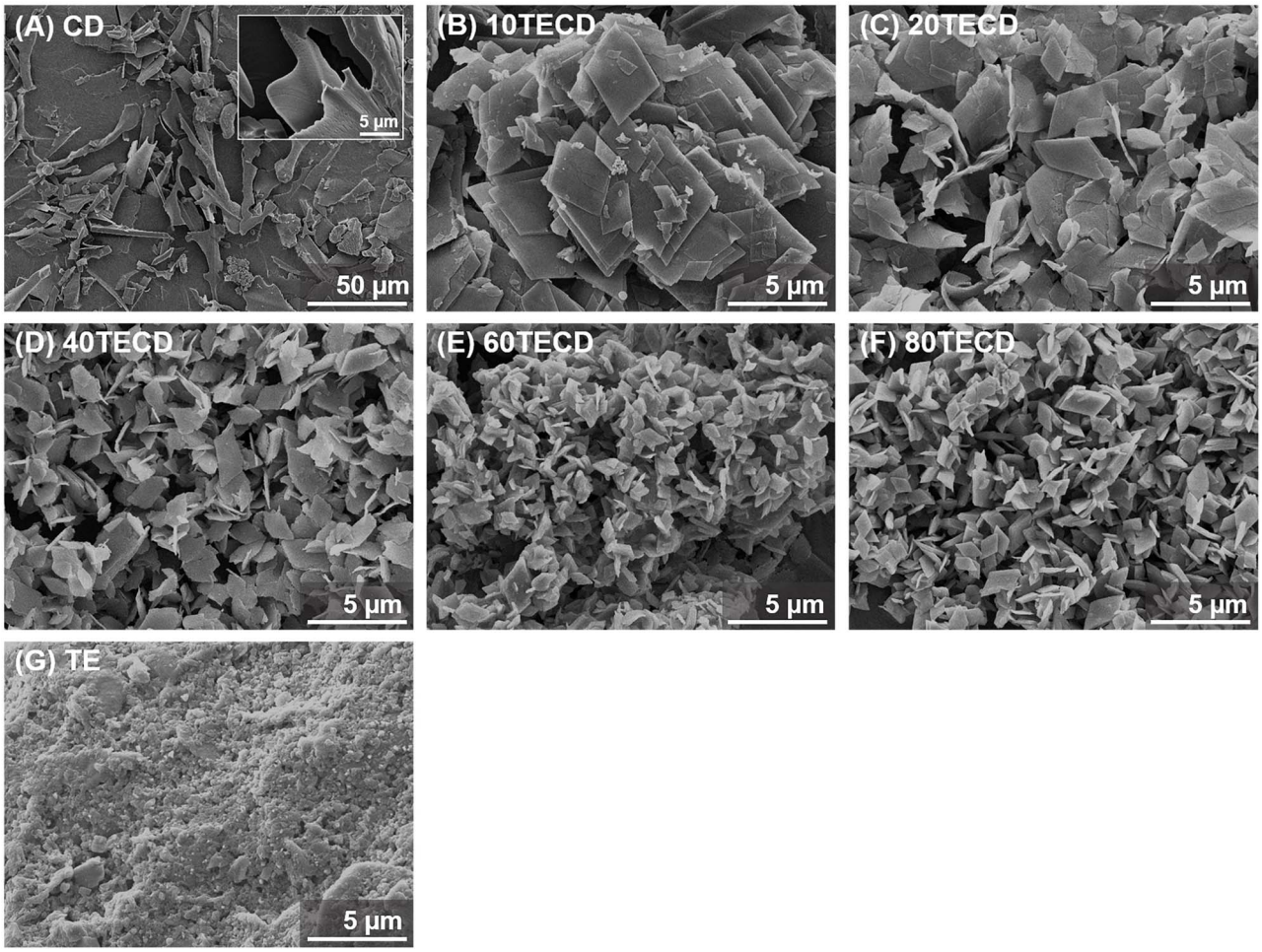

Fig. 3 SEM micrographs showing the surface morphology of: (A) CD powder; (B–F) TECD samples containing TE at different concentrations (10–80 wt%); and (G) TE powder.

increasing initial TE loading, from 0.028 ± 0.002 mg mL^{-1} for 10TECD to 0.115 ± 0.009 mg mL^{-1} for 80TECD (Fig. 2A). This increase contrasts with the constant complexation yield described above, indicating that although excess TE is lost during TECD processing at high loadings, the resulting complexes still contain proportionally more curcumin as the TE input increases. This outcome is consistent with the known selective affinity of cyclodextrins for hydrophobic curcuminoids, which promotes their retention within the TECD complex. UV-VIS measurements showed the same pattern (Fig. 2B), further supporting these observations.

However, aqueous solubility did not follow this linear trend. Instead, solubility peaked at 10TECD (3.25 mg mL^{-1}) and decreased sharply, reaching a constant value of approximately 1.0–1.14 mg mL^{-1} for the 40-80TECD formulations (Table 2). This trend is related to the amount of CD in each formulation, as the outer surface of CD is hydrophilic and contributes to enhancing the aqueous solubility of the inclusion complexes.[11] Higher CD contents result in higher aqueous solubility, since free TE has poor water solubility, and the overall solubility of the complexes is primarily derived from the presence of CD.

3.3. Morphology of TE, CD, and TECD powder

SEM analysis showed distinct morphological differences between the starting materials and the TECD complexes (Fig. 3). The morphology of CD exhibited an irregular flake-like shape (Fig. 3A), whereas TE appeared as small particles (0.11 ± 0.04 μm). For the complexation, a clear morphological transformation was observed. All TECD formulations showed predominantly square, plate-like particles that were markedly different from both starting materials (Fig. 3B–F). The particle size decreased with increasing TE content by 4.7-fold, from 3.69 ± 1.67 μm to 0.79 ± 0.20 μm. This trend reflects a transition from supramolecular CD aggregates formed at low TE loading, where multiple CD molecules self-assemble around a limited number of curcumin molecules, to smaller molecular inclusion complexes at higher TE loading (Scheme 1B), in which most CD molecules are individually occupied by guest molecules.[37] This observation aligns with the TE : CD molar ratios shown in Table 1, which were calculated by assuming a curcumin molecular weight of 368.38 g mol^{-1} and based on the HPLC-determined curcumin content of 16.6% (w/w) in TE. Notably, all TECD particles were substantially larger than TE particles (0.11 μm)

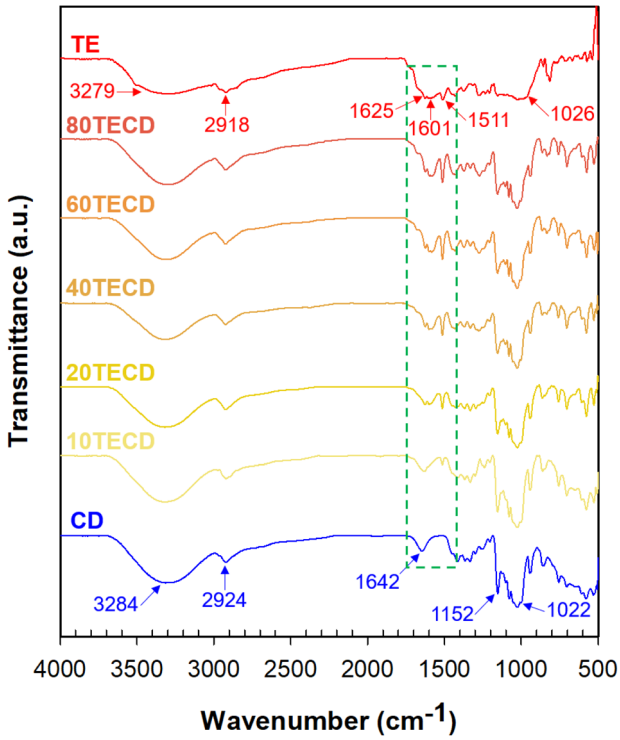

Fig. 4 FTIR spectra of TE, CD, and TECD powders, showing the characteristic peaks of each functional group.

(Fig. 3G), confirming the successful incorporation of TE into CD.

3.4. FTIR analysis of TE, CD, and TECD powder

The molecular interactions between TE and CD and the formation of TECD complexes were confirmed by FTIR analysis (Fig. 4). The characteristic bands of TE powder at 3279, 2918, and 1026 cm^{-1} correspond to O–H stretching, C–H stretching, and C–O–C stretching vibrations, respectively. The bands at 1625 and 1511 cm^{-1} are attributed to symmetric aromatic ring (C=C) stretching and mixed stretching vibrations of C=C and C=O, while the band at 1601 cm^{-1} corresponds to the stretching of benzene ring skeleton. The characteristic bands of CD were observed at 3284, 2924, 1642, 1152, and 1022 cm^{-1}, corresponding to O–H stretching, C–H stretching, H–O–H bending, C–O stretching, and C–O–C stretching vibrations, respectively.[13,37] The FTIR spectra of the TECD powder showed bands corresponding to functional groups of both TE and CD at 3316, 2924, 1627, 1155, and 1026 cm^{-1}. Small shifts in wavenumber were observed, which can be attributed to the host–guest interactions between TE and CD molecules in the inclusion complexes, namely hydrogen bonding and van der Waals interactions.

In addition, the bands at 1601 and 1511 cm^{-1} in the TECD spectra were reduced at lower TE loadings, likely because the guest molecules are shielded within the CD cavity, thereby reducing their interaction with infrared radiation. This observation is consistent with previous reports.[13,28,37] Therefore, these FTIR results qualitatively confirm the successful formation of

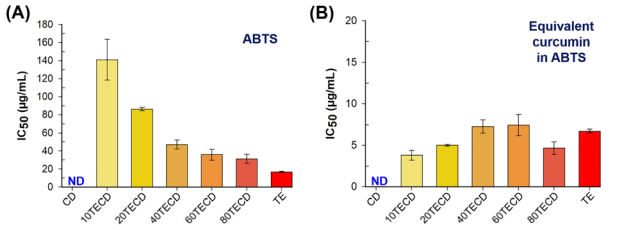

Fig. 5 ABTS antioxidant activity of curcumin in TE and TECD: (A) IC_{50} values of the total complexes, and (B) IC_{50} values based on equivalent curcumin content. ND = Not detected.

inclusion complexes between TE and CD while preserving the chemical characteristics of both the host and guest molecules.

3.5. Antioxidant activity

ABTS assay was selected to evaluate antioxidant activity due to the greater hydrophilicity of the ABTS radical cation ($ABTS^{\bullet+}$), which enables it to penetrate the CD cavity more readily and interact with complexed curcumin.[38,39] The antioxidant activity of TE and each TECD formulation was expressed as IC_{50} values ($\mu g\ mL^{-1}$) (Fig. 5A), which were further converted to curcumin equivalents to compare the relative antioxidant potency of each complex (Fig. 5B). Ascorbic acid was used as the positive control and exhibited an IC_{50} of $5.58 \pm 0.01\ \mu g\ mL^{-1}$.

Free TE exhibited the strongest $ABTS^{\bullet+}$ scavenging activity ($IC_{50} = 16.60 \pm 0.61\ \mu g\ mL^{-1}$), while CD alone showed negligible activity. All TECD complexes showed reduced apparent activity compared to TE, with IC_{50} values decreasing as TE content increased (from 140.91 to 31.31 $\mu g\ mL^{-1}$). At low TE content (10TECD), excess CD promotes the formation of supramolecular assemblies in which curcumin is trapped within multiple CD shells. Although this extensive complexation improves solubility, the number of accessible active sites is limited because only a small fraction of curcumin is actually available for reaction, thereby requiring a higher amount of TECD to achieve a measurable effect. Increasing the TE content shifted the complexes toward smaller inclusion forms, thereby enabling more effective interaction between curcumin and $ABTS^{\bullet+}$.[40]

When normalized to curcumin equivalents, all TECD complexes required similar amounts of curcumin (3.80 ± 0.61 to $7.45 \pm 1.26\ \mu g\ mL^{-1}$) to achieve IC_{50} values comparable to that of free TE ($6.72 \pm 0.25\ \mu g\ mL^{-1}$). These findings demonstrate that TECD complexation preserves the intrinsic radical scavenging capacity of curcumin, which is an essential quality

Table 3 Gel fraction, swelling ratio, and surface pore diameter of PVA hydrogels

Sample	Gel fraction (%)	Swelling ratio	Surface pore diameter (μm)
3PVA	90 ± 3	1.02 ± 0.01	18.87 ± 5.87
5PVA	90 ± 2	1.09 ± 0.01	1.25 ± 0.39
8PVA	88 ± 1	1.20 ± 0.01	2.51 ± 0.89

attribute for therapeutic applications targeting oxidative stress in wound healing.

3.6. Physical properties of PVA hydrogels

The physical properties of PVA hydrogels were determined by gel fraction and swelling ratio measurements (Table 3). Gel fraction represents the percentage of polymer that forms a stable hydrogel network and is commonly used to measure the effectiveness of network formation. All hydrogels showed high gel fraction values, approximately exceeding 90%, indicating a high degree of crosslinking within the hydrogel networks.[41]

The swelling ratio refers to the hydrogel's capacity to absorb and retain water within its polymeric network after irradiation. All hydrogels exhibited swelling ratios slightly above 1, indicating moderate water uptake across the different PVA concentrations. Among them, the 8PVA hydrogel showed the highest swelling ratio, indicating a greater water uptake capacity compared to the 3PVA and 5PVA hydrogels. This behavior can be attributed to the higher PVA content, which may form a more hydrophilic network structure after irradiation, along with its lower initial water content, allowing it to absorb more water when exposed to an aqueous environment. Over time, water continued to diffuse into the hydrogel matrix, reaching near equilibrium by 24 h.

3.7. Mechanical properties of PVA hydrogel

Mechanical testing indicated that tensile properties increased as PVA concentration rose. Specifically, tensile strength values were 15.37 ± 4.38, 35.85 ± 8.04, and 71.94 ± 8.89 kPa for 3PVA, 5PVA, and 8PVA hydrogels, respectively ($p < 0.01$). Elongation at break also increased, with values of 87.09 ± 9.39, 146.07 ± 16.60, and 208.24 ± 14.20% for 3PVA, 5PVA, and 8PVA hydrogels, respectively ($p < 0.01$). However, Young's modulus values for 3PVA, 5PVA, and 8PVA hydrogels were 17.00 ± 5.23, 20.65 ± 2.52, and 22.42 ± 2.32 kPa, respectively, with no statistically significant differences ($p > 0.05$).

The improved mechanical performance with increasing the PVA concentration can be attributed to the formation of a greater number of hydrogen bonds between the hydroxyl groups of the PVA chains after the freeze-thaw process.[42,43] Additionally, the irradiation process randomly introduced chemical crosslinking of PVA chains through free-radical formation.[44] At higher PVA concentrations, the increased availability of polymer chains likely resulted in more reactive free radical sites, leading to a higher crosslink density. Therefore, the combination of higher PVA concentration with both physical and chemical crosslinking mechanisms significantly enhanced the mechanical properties of the PVA hydrogel.

3.8. Morphology of PVA hydrogel

The SEM images exhibited distinct structural differences among the 3, 5, and 8% (w/v) PVA hydrogels, indicating the influence of polymer concentration on network formation and pore structure (Fig. 6A). The 3PVA hydrogel exhibited a highly porous, open-cell structure with large, interconnected pores distributed throughout the matrix in both surface and cross-sectional images, indicating the formation of a loosely crosslinked network. In contrast, the 5PVA hydrogel displayed a denser and smoother surface with only small pores (yellow arrows). The corresponding cross-sectional images (Fig. 6B) showed a transition toward a more compact, layered structure with reduced pore size and fewer open channels compared to the 3PVA hydrogel, suggesting increased polymer chain

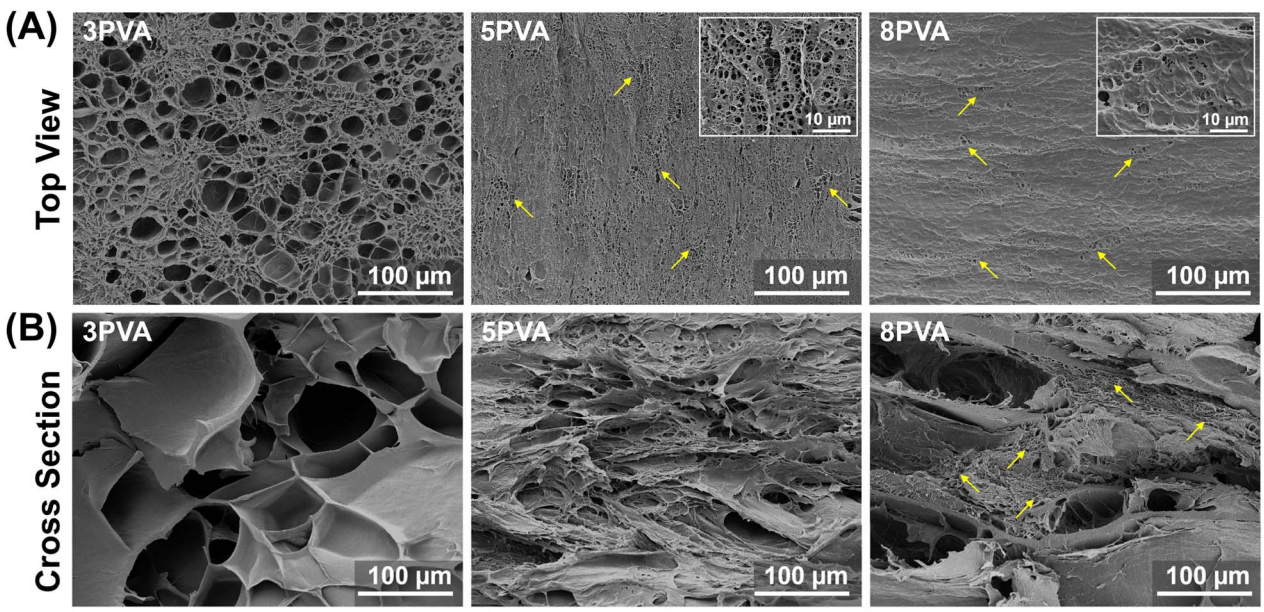

Fig. 6 SEM images of PVA hydrogels prepared at different polymer concentrations: 3PVA, 5PVA, and 8PVA. (A) Top surface morphology; (B) cross-sectional morphology. Yellow arrows indicate small pores observed in 5PVA and 8PVA samples. Insets in the 5PVA and 8PVA surface images highlight the finer pore structures at higher magnification (5000×).

crosslinking during the freeze-thaw cycles and irradiation. With a further increase in polymer concentration to the 8PVA hydrogel, the surface becomes even more compact, with non-uniform visible porosity (yellow arrows). The cross-sectional images show large pores accompanied by smaller micropores (yellow arrows), consistent with a denser and more highly crosslinked network. Therefore, increasing PVA concentration resulted in reduced pore size (Table 3) and lower pore interconnectivity, consistent with previous studies,[45] and leads to a transition from the highly porous structure of the 3PVA hydrogel to the dense, compact network observed in the 8PVA hydrogel.

3.9. *In vitro* curcumin release study and release kinetics

The *in vitro* curcumin release from the 3PVA hydrogel, used as a representative matrix, was investigated to evaluate the impact of different TECD formulations on release behavior. Each 3 × 3 cm^2 hydrogel patch contained 40.5 μg of curcumin equivalent for each TECD formulation prior to the release study (Fig. 7A). In this study, the curcumin was released in the form of TECD. At the early time points (1 and 2 h), the highest cumulative release was observed for the 20TECD formulation, indicating a faster initial burst release. By 6 h, 10TECD followed 20TECD closely, and both formulations maintained higher cumulative release compared to all other formulations through 24 h, while the lowest release was observed with free TE (7.87% at 6 h) ($p < 0.05$) as shown in Fig. 7B. At lower TE loading (corresponding to higher CD content), the aqueous solubility of curcumin was enhanced due to effective inclusion complexation with CD, resulting in faster release during the initial period. In contrast, at higher TE loading, curcumin release was limited by the lower aqueous solubility of the TECD complexes, leading to aggregation of TECD within the hydrogel matrix and restriction of diffusion pathways.[46] Based on its superior early-stage release profile, 20TECD was selected as the optimal formulation for further investigation.

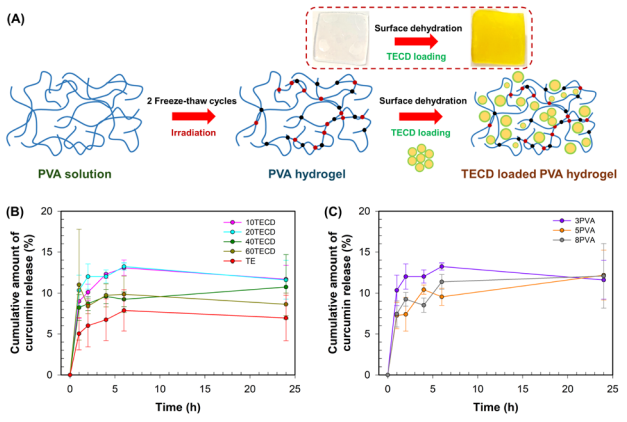

Fig. 7 (A) Schematic illustration of the preparation of PVA hydrogel and TECD-loaded PVA hydrogel. Curcumin release profiles under the effects of: (B) TECD formulations incorporated into a representative 3PVA hydrogel; and (C) PVA hydrogel concentrations loaded with 20TECD.

The 20TECD formulation was selected to investigate the curcumin release as a function of hydrogel matrix concentration. The amount of curcumin released at 6 h from the 3PVA, 5PVA, and 8PVA hydrogels was 13.25%, 11.86%, and 9.54%, respectively, whereas the amount of curcumin released at 24 h was not significantly different ($p > 0.05$) (Fig. 7C). During the first 6 h, the amount of curcumin released decreased with increasing PVA concentration due to the denser polymer network and smaller pore size at higher PVA contents (Fig. 6), as evidenced by SEM analysis, which restricted the diffusion pathway of TECD complexes. This pore size-dependent diffusion behavior is consistent with previous reports on curcumin-pluronic micelle released from hydrogel matrices, in which increasing polymer density reduced pore size and consequently impeded curcumin diffusion.[47] The 3PVA hydrogel reached equilibrium earlier, while the higher PVA hydrogels exhibited delayed but comparable final release amounts. For comparison, the release profiles of the 10TECD formulation across the same hydrogel matrices are provided in Supplementary Fig. S2, further supporting the selection of 20TECD as the optimal formulation due to its consistently superior release behavior. These results indicated that increasing PVA concentration enhances the mechanical properties of the hydrogel, but reduces the initial curcumin release rate.

The release mechanism was further elucidated by fitting the experimental data to the Korsmeyer–Peppas model, which characterizes the release mechanism based on the diffusion exponent (n): (i) Fickian diffusion ($n \leq 0.5$); (ii) anomalous (non-Fickian) diffusion ($0.5 < n < 1$); (iii) case II (time-independent) transport ($n = 1$); and (iv) super case II transport ($n > 1$).[31] All formulations exhibited n values well below the 0.5 threshold, confirming that Fickian diffusion as the predominant release mechanism, whereby curcumin release is primarily driven by concentration gradients with minimal contribution from polymer chain relaxation, swelling-induced convection, or matrix erosion. This behavior is consistent with the high gel fractions (~90%) and stable crosslinked network formed across all hydrogel compositions. The release rate constant, or k, decreased with increasing PVA concentrations, from 0.32 (3PVA) to 0.13 (5PVA) and 0.12 (8PVA), consistent with progressively restricted diffusion in denser polymer networks. The faster release observed for the 3PVA hydrogels containing 20TECD can be attributed to their larger pore size, as reflected by their highest k value among all formulations tested. This system was selected to further investigate cytotoxicity.

In the present system, the capacity of CD to form hydrogen bonds with PVA matrix may simultaneously compete with TECD-water interactions, thereby hindering curcumin diffusion into the release medium, a phenomenon consistent with previously reported findings.[48] To further improve release efficiency, external stimuli such as thermal, ultrasound, or electric fields could be applied to disrupt hydrogen bonding interactions and promote curcumin mobility.[49–51] Compared with similar hydrogel-based curcumin delivery systems reported in the literature, the release profiles observed in this work are consistent with values ranging from 10–25% over comparable timeframes,[46,52] as well as release amounts of 0.2–3.5 μg

reported in related studies.[53] Notably, the enhanced release observed for the 20TECD formulation highlights the advantageous role of CD complexation in improving curcumin dispersion within hydrophilic matrices. Overall, these findings suggest that TECD-loaded PVA hydrogels represent a promising platform for curcumin delivery, performing comparably with previously reported systems while offering potential advantages for wound dressing applications.

3.10. Cytotoxicity test

To assess the biocompatibility of TECD and TECD-loaded hydrogels, cytotoxicity testing was conducted in accordance with ISO 10993-5,[54] which provides standardized guidelines for evaluating the cytotoxicity of medical devices and their materials. Using an MTT-based assay, both TE and 20TECD were evaluated across a concentration range of 7.8–250 μg mL^{-1} to distinguish whether any cytotoxic effects could be attributed to the crude extract or to the TECD complexation. Both TE and 20TECD maintained cell viability within the range of 80–100% across all tested concentrations, comparable to the blank control (culture medium alone), confirming that neither the crude extract nor the complexation process compromised cell viability (Fig. 8A). The 20TECD-loaded hydrogel demonstrated a cell viability of 105.91 ± 5.43%, closely comparable to the negative control (~110%), and in stark contrast to the positive control (~10%), which confirmed a cytotoxic response. This result exceeds the 70% threshold defined by ISO 10993-5 as non-cytotoxic, confirming the cytocompatibility of the hydrogel (Fig. 8B). As the highest cumulative curcumin released from the 20TECD-loaded hydrogel was 13.25%, corresponding to 5.37 μg of released curcumin, this amount remains well below the cytotoxicity threshold observed for the extract alone. Therefore, these results confirm that incorporation of TECD into the PVA matrix at this dosage does not induce adverse cellular responses.

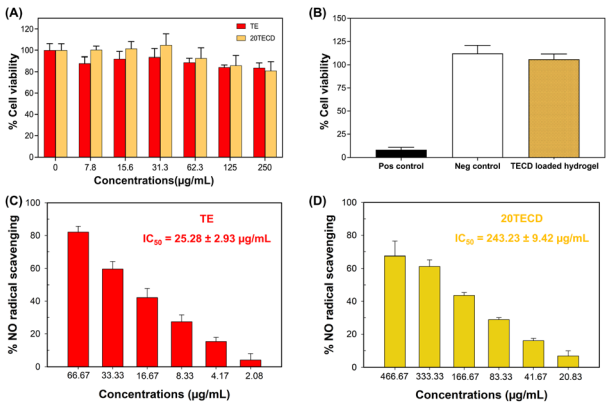

Fig. 8 (A) Cell viability of TE and 20TECD at various concentrations; and (B) cell viability of 20TECD-loaded hydrogel. Pos control refers to the positive control, while Neg control refers to the negative control. NO radical scavenging activity of: (C) TE and (D) 20TECD with corresponding IC_{50} values indicated.

3.11. NO inhibition assay

The anti-inflammatory activity of TE and 20TECD was evaluated through an *in vitro* NO inhibition assay, a widely accepted method for assessing the anti-inflammatory potential of bioactive materials.[33] In this assay, NO radical (NO˙) inhibition was quantified *via* the Griess reaction, which detects nitrite as the end product. A reduction in nitrite levels in the presence of the sample therefore indicates NO˙ inhibition and potential anti-inflammatory activity.[33] The results, expressed as percentage NO radical scavenging as a function of concentration, demonstrated that both TE and 20TECD exhibited concentration-dependent inhibitory activity. The IC_{50} of TE was 25.28 ± 2.93 μg mL^{-1} (Fig. 8C), while 20TECD showed a higher IC_{50} of 243.23 ± 9.42 μg mL^{-1} (Fig. 8D), suggesting a reduction in apparent activity upon complexation, likely attributable to the dilution effect of the CD carrier within the TECD complex. However, when IC_{50} values were normalized to the curcumin equivalent concentration, the values were 10.24 and 14.11 μg mL^{-1} for TE and 20TECD, respectively, indicating that the intrinsic anti-inflammatory activity of curcumin is largely preserved after complexation. Furthermore, CD alone showed no inhibitory effect, confirming that the observed scavenging activity originates from the curcumin rather than the CD carrier. Based on the cumulative curcumin release of 5.37 μg (92.75 μg of 20TECD) from the 20TECD-loaded hydrogel, the released dose corresponds to approximately 30.5% NO˙ scavenging activity, confirming that the released amount remained biologically active and supporting its potential application as an anti-inflammatory wound dressing material.

These findings are consistent with previous studies reporting concentration-dependent NO scavenging activity in curcumin-based systems. For example, Iftikhar *et al.* (2026) reported that nanocurcumin derived from turmeric rhizomes exhibited NO˙ scavenging activity of 55% at 200 μg mL^{-1}, increasing to 92% at 1000 μg mL^{-1}.[55] Similarly, Gouthamchandra *et al.* (2021) evaluated the anti-inflammatory activity of a bisdemethoxycurcumin-enriched turmeric extract (REVERC3) against a regular turmeric extract using the NO inhibition assay, finding inhibitory effects ranging from 10–90% at concentrations of 5–160 μg mL^{-1}, with an IC_{50} of 69.5 μg mL^{-1}. The authors further suggested that REVERC3 reduced nitrite production by disrupting the interaction between NO˙ and oxygen.[56]

4. Conclusions

This study demonstrates that the complexation of TE with CD prior to incorporation into PVA hydrogels significantly improves aqueous solubility and enhances curcumin release. Increasing the TE-to-CD ratio induced a transition from supramolecular assemblies to small-molecule inclusion complexes, achieving greater solubility compared with non-complexed TE. SEM analysis confirmed that higher PVA concentrations produced denser matrices with smaller pore sizes, restricting TECD diffusion and curcumin release, highlighting pore structure as a critical design parameter for tailoring release profiles. The optimized formulation, 20TECD-loaded 3PVA hydrogel,

achieved the highest curcumin release within 6 h, following Fickian diffusion kinetics, demonstrated non-cytotoxicity, and exhibited NO radical scavenging activity. Overall, these findings supported the potential of TECD-loaded PVA hydrogels as bioactive wound dressing materials.

Author contributions

Rawita Morarad: methodology, investigation, formal analysis, writing – original draft. Pennapa Karawak: conceptualization, methodology, writing – review & editing. Pranita Meepean: investigation. Natawan Sritapanya: investigation. Pattaraphorn Panomai: methodology, investigation. Niti Yongvanich: investigation. Pimpon Uttayarat: supervision, conceptualization, writing – review & editing.

Conflicts of interest

There are no conflicts to declare.

Data availability

Data will be made available on request.

Supplementary information (SI): incorporation of TECD in hydrogels; and curcumin release of 10TECD-loaded PVA hydrogels. See DOI: https://doi.org/10.1039/d6ra00713a.

Acknowledgements

This project was sponsored by the Thailand Institute of Nuclear Technology (Public Organization) under grant number 682011401. The morphology of the samples was tested using SEM at the Scientific and Technological Equipment Centre, Silpakorn University.

References

1 S. A. A. Rizvi, G. P. Einstein, O. L. Tulp, F. Sainvil and R. Branly, *Biomolecules*, 2022, **12**, 1442.
2 S. S. Patil, S. Bhasarkar and V. K. Rathod, *Prep. Biochem. Biotechnol.*, 2019, **49**, 407–418.
3 S. J. Hewlings and D. S. Kalman, *Foods*, 2017, **6**, 92.
4 S. Prasad and B. B. Aggarwal, In *Herbal Medicine: Biomolecular and Clinical Aspects*, CRC Press/Taylor & Francis, Boca Raton (FL), 2011, Available from: https://www.ncbi.nlm.nih.gov/books/NBK92752/.
5 R. S. Ahmad, M. B. Hussain, M. T. Sultan, M. S. Arshad, M. Waheed, M. A. Shariati, S. Plygun and M. H. Hashempur, *Evid. Based Complement. Alternat. Med.*, 2020, **2020**, 7656919.
6 M. D. Ciuca and R. C. Racovita, *Int. J. Mol. Sci.*, 2023, **24**, 8874.
7 A. Barzegar, *Food Chem.*, 2012, **135**, 1369–1376.
8 S. I. Sohn, A. Priya, B. Balasubramaniam, P. Muthuramalingam, C. Sivasankar, A. Selvaraj, A. Valliammai, R. Jothi and S. Pandian, *Pharmaceutics*, 2021, **13**, 2102.
9 N. Agrawal and M. Jaiswal, *Eur. J. Med. Chem. Rep.*, 2022, **6**, 100081.
10 J. Górnicka, M. Mika, O. Wróblewska, P. Siudem and K. Paradowska, *Life*, 2023, **13**, 207.
11 V. R. Yadav, S. Suresh, K. Devi and S. Yadav, *AAPS PharmSciTech*, 2009, **10**, 752–762.
12 M. M. Yallapu, M. Jaggi and S. C. Chauhan, *Colloids Surf. B Biointerfaces*, 2010, **79**, 113–125.
13 L. Jiang, N. Xia, F. Wang, C. Xie, R. Ye, H. Tang, H. Zhang and Y. Liu, *LWT - Food Sci. Technol.*, 2022, **171**, 114149.
14 N. Hedayati, M. Montazer, M. Mahmoudirad and T. Toliyat, *Carbohydr. Polym.*, 2020, **240**, 116267.
15 Y. Ding, S. Xu, C. Ding, Z. Zhang and Z. Xu, *Molecules*, 2024, **29**, 1915.
16 S. Pereva, V. Nikolova, T. Sarafska, S. Angelova, T. Spassov and T. Dudev, *J. Mol. Struct.*, 2020, **1205**, 127575.
17 C. Upadhyay, A. D'Souza, P. Patel, V. Verma, K. K. Upadhayay and M. Bharkatiya, *AAPS PharmSciTech*, 2023, **24**, 100.
18 V. Parmar, G. Patel and N. Y. Abu-Thabit, In *Woodhead Publishing Series in Biomaterials, Stimuli Responsive Polymeric Nanocarriers for Drug Delivery Applications*, Woodhead Publishing, Cambridge, 2018, pp. 555–580.
19 A. A. Sandilya, U. Natarajan and H. Priya, *ACS Omega*, 2020, **5**, 25655–25667.
20 J. Li, F. Xu, Y. Dai, J. Zhang, Y. Shi, D. Lai, N. Sriboonvorakul and J. Hu, *Polymers*, 2022, **14**, 5421.
21 N. H. Thang, T. B. Chien and D. X. Cuong, *Gels*, 2023, **9**, 523.
22 S. Khattak, I. Ullah, M. T. Yousaf, S. Ullah, H. Yousaf, Y. Li, H. Jin, J. Shen and H.-T. Xu, *Int. J. Biol. Macromol.*, 2025, **327**, 147270.
23 S. K. Jin, *Chem.–Asian J.*, 2022, **17**, e202200595.
24 Y. Zhong, L. Zhang and Y. Wang, *Front. Chem.*, 2024, **12**, 1376799.
25 Y. Chen, J. Li, J. Lu, M. Ding and Y. Chen, *Polym. Test.*, 2022, **108**, 107516.
26 Y. Zhang, S. Wen, K. Zheng, X. Zhou, C. Huang, Y. Xu, J. Luo and G. Lu, *Biomacromolecules*, 2025, **26**, 5778–5790.
27 R. Pan, G. Liu, Y. Zeng, X. He, Z. Ma, Y. Wei, S. Chen, L. Yang and L. Tao, *Polym. Chem.*, 2021, **12**, 2457–2463.
28 Y. Zhao, C. Dai, Z. Wang, W. Chen, J. Liu, R. Zhuo, A. Yu and S. Huang, *Drug Des. Devel. Ther.*, 2019, **13**, 3269–3280.
29 P. Panomai, S. Thapphasaraphong and N. Nualkaew, *Plants*, 2024, **13**, 2110.
30 R. Chiangnoon, P. Karawak, J. Eamsiri, S. Nuchdang, N. Thamrongsiripak, N. Neramitmansook, S. Pummarin, P. Pimton, K. Nilgumhang and P. Uttayarat, *Gels*, 2023, **9**, 80.
31 R. W. Korsmeyer, R. Gurny, E. Doelker, P. Buri and N. A. Peppas, *Int. J. Pharm.*, 1983, **15**, 25–35.
32 ISO, *Biological Evaluation of Medical Devices—Part 12: Sample Preparation and Reference Materials*, ISO, 2012 10993–12.
33 R. Suksungworn, P. B. Andrade, A. P. Oliveira, P. Valentão, S. Duangsrisai and N. G. M. Gomes, *Int. J. Mol. Sci.*, 2020, **21**, 2421.
34 F. Zsila, Z. Bikadi and M. Simonyi, Miklós, *Org. Biomol. Chem.*, 2004, **2**, 2902–2910.
35 H. H. Tønnesen, M. Másson and T. Loftsson, *Int. J. Pharm.*, 2002, **244**, 127–135.

36 V. S. R. Kotra, L. Satyabanta and T. K. Goswami, *J. Food Sci. Technol.*, 2019, **56**, 5153–5166.
37 P. Arya and N. Raghav, *J. Mol. Struct.*, 2020, **1228**, 129774.
38 R. L. Prior, X. Wu and K. Schaich, *J. Agric. Food Chem.*, 2005, **53**, 4290–4302.
39 A. Floegel, D.-O. Kim, S.-J. Chung, S. I. Koo, O. K. Chun and J. Food Compost, *Anal.*, 2011, **24**, 1043–1048.
40 Y. J. Jo, H. S. Cho and J. Y. Chun, *Food Sci. Biotechnol.*, 2021, **30**, 807–814.
41 E. Halligan, B. S. H. Tie, D. M. Colbert, M. Alsaadi, S. Zhuo, G. Keane and L. M. Geever, *Gels*, 2023, **9**, 439.
42 Y. Mori, H. Tokura and M. Yoshikawa, *J. Mater. Sci.*, 1997, **32**, 491–496.
43 S. Bose, M. A. Khorshidi and C. Lally, *J. Mech. Behav. Biomed. Mater.*, 2025, **161**, 106787.
44 X. Liang, H.-J. Zhong, H. Ding, B. Yu, X. Ma, X. Liu, C.-M. Chong and J. He, *Polymers*, 2024, **16**, 2755.
45 Y. Wiedemann, T. Schmitt, S. Kim, K. Dirnberger, S. Ludwigs and D. J. Lunter, *Eur. J. Pharm. Biopharm.*, 2025, **217**, 114876.
46 B. Braido, Z. Rukavina, Ø. Grimstad, S. Franzè, F. Cilurzo, Ž. Vanić, N. Škalko-Basnet and L. M. Hemmingsen, *J. Drug Deliv. Sci. Technol.*, 2025, **113**, 107380.
47 A. A. Shefa, T. Sultana, M. K. Park, S. Y. Lee, J.-G. Gwon and B.-T. Lee, *Mater. Des.*, 2020, **186**, 108313.
48 I. Ristić, L. Nikolić, S. Cakić, V. Nikolić, J. Tanasić, J. Zvezdanović and M. Krstić, *Gels*, 2024, **10**, 637.
49 C. Huang, S. Wang and H. Yang, *Processes*, 2020, **8**, 172.
50 H. S. Buddhiraju, J. R. Maddilla and A. K. Rengan, *IEEE South Asian Ultrasonics Symposium (SAUS)*, Gujarat, India, 2024, pp. 1–4.
51 K. Huot, R. Morarad, P. Sakunpongpitiporn, S. Niamlang, N. Paradee, N. Parinyanitikul and A. Sirivat, *J. Drug Deliv. Sci. Technol.*, 2024, **97**, 105777.
52 W. Tan, Z. Ma, L. Zhang, M. Zhang, T. Yu, Y. Zhang and T. Zhao, *Polym. Bull.*, 2023, **80**, 9779–9795.
53 D. E. El-Nashar, N. N. Rozik, A. M. Soliman and F. Helaly, *J. Appl. Pharm. Sci.*, 2016, **6**, 67–72.
54 ISO, *Biological Evaluation of Medical Devices—Part 5: Tests for in Vitro Cytotoxicity*, 2009, ISO 10993-5.
55 M. Iftikhar, M. H. D. Othman, I. U. Khan, A. Shehzad, N. J. Ismail, S. H. S. A. Kadir, T. A. Kurniawan, A. F. Ismail, J. Jaafar and M. A. Rahman, *BioNanoSci*, 2026, **16**, 153.
56 K. Gouthamchandra, H. V. Sudeep, S. Chandrappa, A. Raj, P. Naveen and K. Shyamaprasad, *J. Inflamm. Res.*, 2021, **14**, 859–868.